PCM1 labelling reveals myonuclear and nuclear dynamics in skeletal muscle across species

Mark R Viggars, Daniel Owens, Claire Stewart, Catherine Coirault, Abigail L Mackey, Jonathan C Jarvis

PCM1 labelling reveals myonuclear and nuclear dynamics in skeletal muscle across species.

Mark R Viggars[1,2,3], Daniel Owens[1,4], Claire Stewart[1], Catherine Coirault[4], Abigail L Mackey[5,6,7] and Jonathan C Jarvis[1]

[1]Research Institute for Sport and Exercise Sciences, Liverpool John Moores University, Liverpool, UK.

[2]Department of Physiology and Aging, University of Florida, Gainesville, Florida, USA.

[3]Myology Institute, University of Florida, Gainesville, Florida, USA.

[4]Sorbonne Université, INSERM, Myology Research Center, Paris, France.

[5]Institute of Sports Medicine Copenhagen, Department of Orthopaedic Surgery, Copenhagen University Hospital – Bispebjerg and Frederiksberg, Copenhagen, Denmark.

[6]Center for Healthy Aging, Xlab, Department of Biomedical Sciences, Faculty of Health and Medical Sciences, University of Copenhagen, Copenhagen, Denmark.

[7]Department of Clinical Medicine, University of Copenhagen, Copenhagen, Denmark (Part of IOC Research Center Copenhagen).

Corresponding authors:

Correspondence to: Mark Viggars m.viggars@ufl.edu ORCID: 0000-0002-0722-7051

Physical Address: Department of Physiology & Aging, University of Florida, Gainesville, Florida United States.

and Jonathan Jarvis J.C.Jarvis@ljmu.ac.uk ORCID: 0000-0001-8982-6279

Physical address: School of Sport and Exercise Science, Liverpool John Moores University, Byrom St Liverpool L33AF, UK

Short Title: PCM1 in skeletal muscle nuclei

Keywords: hypertrophy, regeneration, laminopathy, myonuclei, skeletal muscle, satellite cell, pericentriolar material-1, macrophage.

Conflict of interest: The authors declare no conflicts of interest.

ABSTRACT:

Myonuclei transcriptionally regulate muscle fibers during homeostasis and adaptation to exercise. Their cellular location and quantity are important when characterising phenotypes of myopathies, the effect of treatments and to understand the roles of satellite cells in muscle adaptation and muscle 'memory'. Difficulties arise in identifying myonuclei due to their proximity to the sarcolemma and closely residing interstitial cell neighbours. We aimed to determine to what extent PCM1 is a specific marker of myonuclei *in-vitro* and *in-vivo*. Single isolated myofibers and cross-sections sections from mice and humans were studied from several models including Wild-type and Lamin A/C mutant mice after functional overload, and damage and recovery in humans following forced eccentric contractions. Fibers were immuno-labelled for PCM1, Pax7 and DNA. C2C12 myoblasts were also studied to investigate changes in PCM1 localisation during myogenesis. PCM1 labelled the nuclear envelope of myonuclei in mature myofibers and in newly formed myotubes, but also labelled centrosomes in proliferating myogenic precursors which may or may not fuse to join the myofiber syncytium. It also labelled non-myogenic nuclei near the sarcolemma especially in regenerating areas of the *Lmna*$^{+/\Delta K32}$ mouse and damaged human muscle. While PCM1 is not completely specific to myonuclei, the impact that PCM1+ macrophages and interstitial cells have on myonuclei counts would be small in healthy muscle. PCM1 may prove useful as a marker of satellite cell dynamics due to the distinct change in localisation during differentiation, revealing satellite cells in their quiescent (PCM1-), proliferating (PCM1+ centrosome), and pre-fusion states (PCM1+ nuclear envelope).

INTRODUCTION:

Myonuclei influence transcriptional activity within myofibers in response to changes in activity or loading(1). The large cytoplasmic volume of myofibers is maintained by multiple post-mitotic myonuclei regularly distributed along the sarcolemma(2), except at specialised regions such as the myotendinous junction(3) and neuromuscular junction(4). Changes in their distribution and number (through satellite cell (SC) fusion or myonuclear loss), is of key importance in understanding muscle adaptation to age(2), supraphysiological loading/growth(5-9), or exercise(10-12), and whether an increased number of nuclei per fiber can be retained over long periods to support faster muscle growth when re-training or recovering from catabolic episodes such as disuse(8, 11, 13-15). Several studies show that the skeletal muscle epigenome can be altered, potentially allowing for accelerated muscle growth after previous training episodes(16-19), but it is still disputed whether

the maintenance of an increased number of myonuclei is a potential cellular adaptive mechanism enabling rapid re-growth(8). Myonuclear maintenance is also important in myo/laminopathies, such as Lamin A/C deficiency, in which faulty nuclear mechanics and impaired mechanically-activated gene transcription lead to severe muscle dystrophy and skeletal muscle weakness(20, 21).

Myonuclei are generally spindle shaped, with a long axis of 20-30µm and short axis of 6-10µm. On transverse cryosections, typically 5-12µm thick, it becomes a challenge to differentiate between myonuclei and other nuclei that reside underneath the endomysium without automated approaches(22-25). Labelling with dystrophin/laminin reveals whether a nucleus resides inside the sarcolemma (myonucleus), between the basal lamina and sarcolemma (SC nucleus), or outside the basal lamina (stromal/vascular cell nucleus), and determination of this position can be automated during image analysis(24, 25).

To identify myonuclei more reliably than through the positioning of DAPI relative to sarcolemmal labelling, Winje *et al*.(26) reported that a pericentriolar protein, pericentriolar material-1 (PCM1), can be used as a specific marker for myonuclei in skeletal muscle tissue. PCM1 prepares a cell to divide and supports the stability of centrosomes during mitosis(27-29). PCM1 relocalises to the nuclear envelope (NE) of post mitotic nuclei, giving a ring appearance when nuclei are cut in thin transverse sections. However, PCM1 is ubiquitously expressed and may thus be present in all cell types within skeletal muscle tissue(30).

Therefore, to make an independent assessment of PCM1 as a marker of myonuclei in a more varied set of samples, we extracted single myofibers, myofiber bundles, as well as transverse sections to assess the localisation and cell cycle stage of the nuclei within and near myofibers. We analyzed mouse fibers following synergist ablation overload (functional overload) in WT and *Lmna*$^{+/\Delta K32}$ mice and human fibers following eccentric damage and recovery after electrical activation during imposed muscle stretch. We also investigated PCM1 localisation during maturation in C2C12 myoblasts/myotubes. Our objective was to elucidate whether PCM1 antibody labelling can be used on skeletal muscle cross-sections as a specific marker of myonuclei in any case, or whether the protein may be expressed in proliferating myogenic, interstitial, or inflammatory cells. We hypothesised that models of overload and regeneration that greatly expand the SC pool may be the most affected and vulnerable to overestimation of myonuclear number.

METHODS:

Mouse C2C12 Cell Culture

C2C12 murine skeletal myoblasts(31, 32), from ATCC®, (Virginia, United States), were incubated on gelatin (0.2%) coated plastic cover slips in 12 well-plates in humidified 5% CO_2 at 37°C in 1ml growth medium (GM) containing DMEM, 10% FBS, 10% NCS, 1% l-glutamine (2mM final) and 1% penicillin–streptomycin solution. Upon reaching confluence, cells were fixed with 0.5% PBS/BSA containing 2% paraformaldehyde or, to produce multinucleated myotubes, myoblasts were differentiated by washing with PBS and transferring to low serum media (LSM; DMEM with 2% horse serum, 1% l-glutamine and 1% penicillin–streptomycin). C2C12 cells spontaneously differentiate under these conditions without additional growth factors(31) and were fixed after 7-days in LSM.

Fixed cells were incubated with a cocktail of antibodies/dyes including anti-PCM1 (HPA23370 Sigma Aldrich, Merck) at 1:1000 and Phalloidin-FITC (Sigma P5282) at 1:500 overnight in immunobuffer (IB): PBS (10mM phosphate pH-7.4, 150mM NaCl), 50mM glycine, 0.25% BSA, 0.03% saponin, 0.05% sodium-azide. An appropriate secondary antibody for anti-PCM1, Goat Anti-Rabbit IgG-Alexa Fluor®594) (ab150077) was added 1:1000 the following day in IB. Following labelling, the plastic coverslips were removed, blotted dry and placed on glass slides in mounting medium (Vectashield® with DAPI (1.5µg/ml), Burlinghame, CA, USA) before imaging. Experiments were performed at 3 different passages (5, 8, 11) and images taken from random regions of interest comprising 3 technical replicates.

Human Eccentric Damage and Recovery

The Regional Scientific Ethical Committees of Copenhagen in Denmark approved this study (Ref: HD-2008-074) and all procedures conformed to the Declaration of Helsinki. Young, healthy males (*n*=2), age; 20.5± 0.5 years, height; 1.78± 0.02 cm, body mass; 76.5± 1.5 kg) gave informed consent and underwent a muscle injury protocol of 200 forced lengthening contractions with electrical stimulation to activate the target muscle during each contraction, as previously described (33). The protocol was performed on the vastus lateralis muscles of one leg, leaving the other as internal control. The muscle biopsies analysed here are a subset of samples from participants in whom extensive muscle damage was previously observed (33, 34).

Muscle biopsies were collected from both vastus lateralis muscles immediately before the damaging exercise and at 2, 7 and 30-days from the damaged leg thereafter. Biopsies were taken under local anaesthetic (1%

lidocaine: Amgros I/S, Copenhagen, Denmark), using the percutaneous needle biopsy technique of Bergström (35), with 5–6-mm-diameter biopsy needles and manual suction.

On extraction, biopsies were prepared for histology and single fiber analysis as previously described(34). Single fibers bundles were pinned to maintain fiber length and covered in Krebs-Henseleit bicarbonate buffer (containing 0.1% procaine) for 2 minutes, followed by Zamboni fixative (2% formaldehyde, 0.15% picric acid) for 30 min, then transferred into fresh Zamboni fixative and placed in the fridge for approximately 4 hours. Zamboni fixative was then replaced with 50% glycerol in PBS and moved to -20°C on the following day until extraction.

Functional overload of the mouse plantaris

8 Wildtype (WT) and 10 *Lmna*$^{+/\Delta K32}$ mice used in previous analyses(36) were included in this study and underwent a sham operation or functional overload (FO) of the plantaris muscles, by aseptic tenotomy of soleus and gastrocnemius muscles in both hind limbs(37). The cut distal tendons were folded proximally and sutured to the proximal musculotendinous region leaving the plantaris intact. Animals recovered within 1-2 hours and were provided analgesia prior to and following surgery (Vetergesic© 0.3 mg/ml, SC:0.10mg/kg).

After 1-week of FO or sham surgery, animals were sacrificed by cervical dislocation, plantaris muscles were dissected, and visible fat and connective tissue removed. Isolated plantaris muscles were frozen in isopentane above liquid nitrogen for histological analysis or fixed in 4% paraformaldehyde at room temperature for one hour for analysis of single muscle fibers. After fixation, PLN muscles were placed on ice and sucrose solution was added in increasing molarity (0.5mM, 1mM, 1.5mM) and then frozen at -80°C in 2mM sucrose. Sucrose frozen fibers were later placed on ice and transferred through decreasing molarity sucrose into IB for mechanical isolation.

Immunolabelling and analysis of single fibers and cross-sections.

Single fibers were teased from fiber bundles under a stereomicroscope in IB. In some instances, mouse fibers were extracted in bundles due to their small size and fragility during manual dissection. Primary antibody cocktails of Pax7 (DSHB supernatant, 1:100) and anti-PCM1 (1:1000) were added to the petri dish in IB + plus 0.2% Triton-X100 overnight and then washed 3 x 10 minutes in IB. Secondary antibodies (Goat anti-mouse IgG-Alexa Fluor®488 (ab150113) and Goat anti-rabbit IgG-Alexa Fluor®594 (ab150077) were added at 1:1000 in IB

for 2 hours before 3 x 10 minute washes in IB, before single fibers were mounted in DAPI (Vectashield® with DAPI) onto glass slides before cover slipping and imaging.

For muscle cross-sections, snap-frozen muscle was sectioned at 10µm using an OTF5000 Cryostat (Bright Instruments, UK) onto ThermoScientific™ SuperFrost Plus™ Adhesion slides (ThermoFisher Scientific Inc, USA). Immunostaining and cover slipping were completed as above on glass slides, but adding antibodies anti-collagen IV AB769 (Merck, Germany) at 1:500 and anti-CD68 MO718 (Dako, Denmark) at 1:500 for human cross-sections. Secondary antibodies were donkey anti-goat Alexa Fluor®680 (a-21084) and donkey anti-mouse Alexa Fluor®488 (ab150109) respectively at 1:1000 diluted in IB. A DSHB supernatant was used for dystrophin on mouse sections MANDYS8 8H11 at 1:100 (DSHB deposited by Morris, G.E.), combined with a goat anti-mouse IgG H&L Alexa Fluor®594 preadsorbed (ab150120) secondary antibody at 1:500 in IB.

Imaging, PCM1 localisation and myonuclear analyses

Cells/myofibers were imaged under 20x magnification and 30µm Z-stacks produced with 3µm steps using a widefield fluorescent microscope (Leica DMB 6000, Germany) to determine PCM1 presence and localisation. An A4 filter cube was used to image DAPI (EX: 340-380, EM: 450-490), L5 filter cube to image FITC and Alexa Fluor® 488 (EX: 460-500, EM: 512-542) and an RHO filter cube to image Alexa Fluor®568/594 (EX:541-551, EM:565-605). Images were taken with a monochrome DFC365 FX camera (Leica, Germany) and fluorescent channels overlayed to determine PCM1 and Pax7 localisation. The number of Pax7+ cells per myofiber (not normalised to fiber/sarcomeres per mm), and the percentage of Pax7+ cells that also displayed PCM1 positivity were quantified on single myofibers from humans and mice across all timepoints and conditions. Manual Pax7+ cell identification was performed on human cross-sections from control and 7-days after eccentric damage, noting Pax7+ cells that were also PCM1+. Myonuclei identification was performed using DAPI and a sarcolemmal marker, identifying myonuclei as nuclei whose centroid was clearly within the sarcolemmal labelling. A second manual analysis was performed using PCM1 with sarcolemmal labelling to identify PCM1+ nuclei within the sarcolemmal boundary as above, as well as the total number of PCM1+ nuclei independent of localisation to the sarcolemma. These measures and total DAPI+ nuclei were counted manually using the multi-point tool on single fields of view using Image Jv1.53(38).

Statistics

Data were analyzed using GraphPad Prism 8 (GraphPad Software, San Diego, CA, USA). Comparisons of PCM1 localisation *in-vitro* after 2 and 7 days in LSM was performed using a one-way ANOVA with Tukey's post hoc testing. The number of Pax7+ cells per muscle fiber and the % of PCM1+ Pax7+ cells from human and mouse isolated myofibers were also compared by one-way repeated measures ANOVA with Tukey's post-hoc testing. Paired t-tests were performed to compare nuclear characteristics between control and 7-days post eccentric damage on muscle cross-sections in humans. Bland-Altman analysis was performed using GraphPad Prism 8 software on the comparison of PCM1 labelling of myonuclei (subsarcolemmal PCM1) to manual quantification of myonuclei through their subsarcolemmal positioning in control and 7-days post damage on human transverse cross-sections. This analysis was also performed comparing myonuclei per fiber cross-section measurements to manual quantification of all PCM1+ nuclei for WT & $LMNA^{+/\Delta K32}$ control mice and after functional overload.

RESULTS:

PCM1 localisation changes consistently during C2C12 myoblast proliferation and differentiation into myotubes *in-vitro*.

As previously reported(39), PCM1 is present at the centrosome during proliferation in C2C12 mouse muscle cells *in-vitro* (Figure 1A, C). When myoblasts are transferred to low serum media, a differentiation programme is initiated in which PCM1 re-localises to form a perinuclear matrix around the myoblast nuclei seen as NE staining, (Figure 1B). This change in localisation occurs during differentiation, preceding fusion of the myoblasts into a multinucleated myotube(39). After 2-days in LSM, 75.7 ± 9.3% of nuclei had PCM1+ centrosomes, with a significantly lower amount (17.5 ± 9.2%, P <0.0001) of nuclei with PCM1+ NEs (unfused). There was a small population of already fused cells with PCM1+ NEs (6.8 ± 3.3%), significantly lower than the population of cells with PCM1+ centrosomes (P <0.0001), and populations of cells with PCM1+ NEs that had differentiated but not yet fused, (P <0.019), Figure 1E. Following 7-days in LSM, only 16.6 ± 7.1% of nuclei had PCM1+ centrosomes and 11.6 ± 4.1% of cells had PCM1+ NEs but remained visibly unfused. There were significantly more nuclei with PCM1+ NEs that had undergone fusion, 71.8 ± 7.3% which was significantly higher than the remaining populations of nuclei, <0.0001, Figure 1F.

This change in PCM1 localisation may be required for appropriate cytoskeletal reorganisation, as motor proteins pull two myoblasts together before fusion(4). Once fused, PCM1 remains present at the NEs in the myotube, (Figure 1B/D). These results were also replicated in human primary cells, with similar observations during proliferation and early differentiation as seen in C2C12 cells (Data not shown).

Insert Figure 1 Here

Human skeletal muscle degeneration and regeneration reveals multiple PCM1+ cell populations.

We examined single muscle fibers/fiber bundles and transverse sections from human vastus lateralis biopsies taken before and 2, 7 and 30-days after eccentric damage, a model that has been shown to produce myogenesis in adult skeletal muscle(33, 34). On cross-sections, PCM1 labelling of myonuclei at the NE can appear either as a hollow ring, or as a single spot depending on where the nucleus is sectioned, (Figure 2A). On single fibers, PCM1 labelling of myonuclei appears mainly as a hollow ring, (Figure 2B-C). PCM1 protein was identified on some Pax7+ cells on both cross-sections (Figure 2A) and single isolated myofibers, (Figure 2C). Quantification of Pax7+ cells per fiber was performed revealing a significant increase in their number 7-days post eccentric damage (5.9 ± 5) compared with control (3.1 ± 2.2, $P = 0.0002$) and 2-days post damage (3.7 ± 2.5, $P = 0.0077$). The percentage of Pax7+ cells that also exhibited PCM1 positivity at their centrosome or NE was 9.5 ± 1.5% in the control state and increased at 2-days (20 ± 3%, *P = 0.14),* before peaking at 7-days (29.5 ± 3.5%, *P = 0.01*) post damage (Figure 2E). PCM1+/Pax7+ cells remain slightly elevated at 30-days post damage compared to baseline (18.5% ± 3, $P = 0.18$), with some Pax7+ cells exhibiting PCM1+ NEs which we believe are myocytes or pre-fusion cells, replicating our *in-vitro* observations of PCM1 stage-specific localisation.

Insert Figure 2 Here

We also manually quantified the number of myonuclei, PCM1+ myonuclei, total PCM1+ nuclei, Pax7+/PCM1-, Pax7+/PCM1+ and all DAPI+ nuclei (measurements are per fiber) on cross-sections from the same biopsies as the single fiber analysis. We selected to compare cross-sections from control and the 7-days post eccentric damage timepoint as this displayed the greatest amount of cellular remodelling(34). This analysis was performed on 2 participants, using 4 random images per biopsy, per timepoint, Table 1.

Table 1: Assessment of nuclei populations on human muscle cross-sections in control and muscle 7-days post eccentric damage. *Data is shown from 2 individuals. *Indicates a significant difference ($p = 0.05$).

Per Fiber Cross-Section	**Control**	**7-Days Post Damage**	***P*-Value**
Pax7+ Nuclei	0.16 ± 0.03	0.17 ± 0.04	0.7
Pax7+/PCM1+	0.06 ± 0.02	0.09 ± 0.01	**0.036***
Myonuclei (DAPI + Sarcolemmal Positioning)	2.04 ± 0.15	2.01 ± 0.08	0.827
PCM1+ Myonuclei	2.1 ± 0.17	2.16 ± 0.08	0.679
Total PCM1+ Nuclei	2.92 ± 0.5	3.89 ± 0.84	0.094
Total DAPI + Nuclei	4.43 ± 0.94	7.03 ± 2.27	**0.048***

This analysis was extremely difficult in damaged/necrotic fibers due to the large density of nuclei within the cytosol which is more easily seen on extracted myofibers (Figure 3A-B). While Pax7+ nuclei per fiber cross-section did not differ between conditions (0.16 ± 0.03 vs. 0.17 ± 0.04, *P* = 0.7), the number of Pax7+/PCM1+ SCs was higher (0.06 ± 0.02 vs. 0.09 ± 0.01, *P* = 0.036) 7-days post eccentric damage. There was no difference pre and post intervention in either manual counts of myonuclei (sub-sarcolemmal DAPI labelling) (2.04 ± 0.15 vs. 2.01 ± 0.08, *P* = 0.83), or PCM1+ myonuclei counts (sub-sarcolemmal PCM1 labelling) per fiber cross-section 2.1 ± 0.17 vs. 2.16 ± 0.08, *P* = 0.7). Bland-Altman analysis was performed and reported good agreement between manual counting of myonuclei through DAPI labelling with sub-sarcolemmal positioning, versus PCM1 immunolabelling of myonuclei with subsarcolemmal positioning with 95% limits of agreement of -0.24 and 0.44. There was a slight bias (0.099 ± 0.17) toward PCM1 labelling reporting higher myonuclei numbers versus manual counting as previously reported(15, 26), but both fell within agreement, Supplementary Figure 1. However, 7-days post damage, there was a trend suggesting an increase in reported PCM1+ nuclei, despite no change in PCM1+ myonuclei which is probably because of proliferating interstitial cells (2.92 ± 0.5 vs. 3.89± 0.84, *P* = 0.094). The total number of DAPI+ nuclei did increase 7-days post damage, (4.43 ± 0.94 vs. 7.03 ± 2.27, *P* = 0.048), likely reflecting the increase in infiltrating cells and interstitial nuclei(34, 40).

At 7-days, it can be observed on both cross-sections and isolated myofibers that there is extensive necrosis and infiltration of other cell populations into damaged myofibers. Many of these cells within necrotic zones

have distinctive PCM1+ centrosomes and lay adjacent to intact fibers (indicated with an asterisk, Figure 3A-B, Figure 4A-C). Using the same human biopsy material, it has previously been reported that these zones are full of immune cells (CD68+) that infiltrate and remove severely damaged myofibers(34). Here we show that CD68+ infiltrating cells also express PCM1 and appear across the entire damaged cytoplasm, or near to myonuclei that remain at the basement membrane, Figure 4A-C. We also highlight that interstitial space in skeletal muscle contains cells with PCM1+ NEs and cells with PCM1+ centrosomes near the myofiber boundaries (Figure 2) which is exacerbated after damage (Figure 4).

Insert Figure 3 Here

Insert Figure 4 Here

Defective muscle plasticity in *Lmna*$^{+/\Delta K32}$ mutant mice following mechanical overload is accompanied by higher numbers of PCM1+ Pax7+ cells and impaired nuclear spreading in-vivo.

We recently reported(36) that under basal conditions WT and *Lmna*$^{+/\Delta K32}$ mutant plantaris muscles are equivalent in mass (WT = 0.69 ± 0.02mg.g^{-1} vs. *Lmna*$^{+/}$ΔK32 = 0.65 ± 0.02mg.g^{-1}). Following 1-week of mechanical overload, WT muscles make a robust hypertrophic response (1.15 ± 0.07mg.g^{-1}), but the mutant presents defective hypertrophy (0.84 ± 0.05mg.g^{-1}). This reduced response to mechanical overload is accompanied by defective myonuclear accretion, nuclear deformity, and an increase in both Pax7+ cells and EdU+ fibers inside and outside of the myofiber (36). These adaptations and developed muscle pathologies can be visualised in Figure 5A-E, with more data available in a recent publication by Owens *et al.*(36).

Insert Figure 5 Here

While we have previously reported an increase in satellite cells on cross-sections in response to functional overload, our assessment on single fibers showed minimal difference in the number of Pax7+ cells per fiber (not normalized to fiber length) between conditions, WT sham (2.58 ± 0.25), WT functional overload (2.99 ± 0.42), *Lmna*$^{+/}$ΔK32 sham (1.96 ± 0.31), and *Lmna*$^{+/}$ΔK32 functional overload (2.58 ± 0.6), Figure 6F. This analysis was performed by counting Pax7+ cells on 39 ± 3, 52 ± 7, 36 ± 4, 41 ± 7 muscle fibers per group respectively. This discrepancy may be explained by the fact that damaged/regenerating fibers that typically have more Pax7+ cells in their proximity were more likely to break during mechanical isolation and were therefore not

successfully extracted and imaged. There was a small significant increase in the number of Pax7+ cells per fiber between WT functional overload muscles and *Lmna*$^{+/}$ΔK32 sham muscles (*P* =0.026).

We then sought to assessed PCM1 localisation on Pax7+ cells in this extensive muscle pathology where regeneration and proliferative cells are common. From the single isolated myofibers assessed here, the number of PCM1+ Pax7+ cells are comparable at baseline in WT (8 ± 3.55%) and mutant (8.75 ± 5.9%, *P* = 0.99), (Figure 6A, C). After overload, the percentage of PCM1+ Pax7+ cells were similar to sham muscles in the WT but some individual samples showed that there was likely extensive proliferative activity through increased PCM1+ Pax7+ cells (16 ± 6.65%, *P* = 0.337), Figure 6B). We identified a significant increase in the mutant (22 ± 7.89%, *P* = 0.02) vs the WT sham control (Figure 6D). We also highlight that myotubes forming in the *Lmna*$^{+/\Delta K32}$ mutant after overload had more closely chained myonuclei (Figure 6E), characteristic of earlier development. Conversely, myotubes present in WT exhibit appropriate nuclear spreading and peripheral migration (Figure 6B). The lack of or delay in this behaviour may be an additional factor contributing to defective hypertrophy previously reported(36).

Lastly, we sought to identify the extent to which counting only PCM1+ nuclei would bias 'myonuclei' counts across all for conditions in the mouse. Bland-Altman analysis comparing MyoVision myonuclei per fiber cross-section measurements (previously reported(36)) with manual quantification of all PCM1+ nuclei, showed that in all instances there was a bias in that counting all PCM1+ nuclei overestimated myonuclear number when assessed by DAPI positioning relative to the sarcolemma using an automated, unbiased software programme. This was most obvious in WT & *Lmna*$^{+/\Delta K32}$ mutants (-0.18 vs -0.14) and increased 7-days post functional overload (-1.18 vs -1.83) and 14-days post functional overload (-0.81 vs -0.53) due to the cellular proliferation in the hypertrophying and regenerating muscles, (Supplementary Figure 2).

Insert Figure 6 Here

DISCUSSION:

Bergmann and colleagues first identified PCM1 in the NE of mature cardiomyocytes(41, 42). The Gundersen laboratory later elegantly investigated PCM1 as a potential gold standard marker of myonuclei in skeletal muscle from mice, rats, and humans(26). However, PCM1 is reportedly ubiquitously expressed at the pre-mRNA level independent of cell lineage during mitosis, and is expressed in a range of cells as well as myofibers,

including schwann, immune, fibro-adipogenic, and endothelial cells, and in smooth muscle, tenocytes, SCs and motor neurons/neuromuscular junction nuclei across multiple muscles, developmental stages and adulthood, as assessed through single-nuclei RNA sequencing(30, 43). We observed the localisation of PCM1 within several relevant models (WT mice, *Lmna*$^{+/\Delta K32}$ mice and humans). Anti-PCM1 does label certain Pax7+ cells at the centrosome, while previous reports have suggested it is specific to myonuclei(26). The pattern of labelling in SCs is distinctively different to that in myonuclei, localizing to poles of the SC centrosome rather than the NE, as seen in myonuclei. The percentage of PCM1+ SCs was dependent on the regenerative state and model used leading to the proposal that such non-myonuclear immunolabelling reflects the extent of proliferative expansion of interstitial cells most obviously in regenerating muscle. The number of Pax7+/PCM1+ cells increase in human cross-sections and single fibers 7-days post eccentric damage and in *Lmna*$^{+/\Delta K32}$ mice following functional overload, but not to a significant extent following functional overload in WT mice.

There are distinct changes in PCM1 localisation both *in-vitro* and *in-vivo* that represent cell cycle stages of SCs; first at the centrosome during prophase or anaphase, and then at the NE, when PCM1 forms an insoluble perinuclear matrix as the nucleus exits the cell cycle into G0 to prepare for fusion into differentiated myotubes(39, 44, 45). The change in PCM1 localisation from centrosome to NE occurs in single muscle cell precursors and precedes fusion of two mononucleated cells into a myotube (Figure 1). This change in PCM1 localisation may be required for appropriate cytoskeletal reorganisation, as motor proteins pull two myoblasts together before fusion(4). Single mononucleated Pax7+ cells with PCM1+ NEs we believe are indicative of 'pre-fusion' cells. Srsen *et al.* previously reported that all Ki67+ proliferating myoblasts were also PCM1+ at the centrosome and that upon PCM1 relocalisation to the NE, Ki67 positivity was lost(39). It has previously been reported that such mononucleated cells with PCM1+ NEs express both embryonic myosin and myogenin which are upregulated during differentiation(39). PCM1 may thus prove useful as a marker of the *in-vitro* cell cycle and fusion index of myotubes due to a distinct change in localisation during differentiation.

PCM1 was also found in connective tissue/interstitial nuclei and within regenerating and necrotic myofibers in nuclei that belong to proliferating macrophages. With this in mind, we advise caution on identifying all PCM1 labelling as indicative of myonuclei in skeletal muscle, without clear confirmation of sub-sarcolemma positioning and the distinctive perinuclear patterning. Determining the number of non-myonuclei which are PCM1+ is therefore important, especially if automated counting or subjective microanatomical analysis is

performed. From previous analyses, the number of myonuclei per fiber cross-section in mature skeletal muscle ranges between 1.5 and 4.5, and for every 100 myonuclei there are about 1-5 SCs, or 0.04-0.25 Pax7+ cells per fiber cross-section, depending on species, age, predominant fiber type composition, tissue section thickness and the geometrical inclusion criteria to define a myonucleus(8, 26, 46-51). This means that the differences in SC PCM1 positivity across our models would probably not affect overall myonuclei counting with PCM1 and would be of minimal concern in healthy muscle and will be a valuable tool going forward in most instances. However, we show a trend for an increase in total PCM1+ nuclei 7-days post eccentric damage in humans (~33%, P = 0.094), which would probably reach significance in an appropriately powered experiment. In addition, two studies have reported and noted higher myonuclei per fiber cross-section values (~11-16%) when labelling with PCM1 in comparison to conventional positional methods[26,52], so we advise labs to independently assess whether PCM1 is suitable for myonuclear counting depending on their muscle phenotype, and especially if small differences between myonuclear number are to be expected between conditions. Our investigation was performed across species and models but on small sample sizes. Therefore, data presented may not be fully representative of whole muscles but highlights several cell populations other than myonuclei that can be PCM1 positive within skeletal muscle.

While perinuclear PCM1 is not entirely specific to myonuclei, the impact of other PCM1+ nuclei would have little effect on total myonuclei counts in most physiologically relevant models of hypertrophy yet may be problematic in regenerative models or myo/laminopathies where there are more PCM1+ infiltrating macrophages and interstitial cells. We suggest the use of PCM1, Pax7 and a basement membrane marker to make completely sure the PCM1 labelling is associated with the perinuclear labelling of the myonucleus. PCM1 may also prove useful as a marker of both *in-vitro and in-vivo* SC dynamics due to the distinct change in localisation during differentiation which reveals SCs in their quiescent (PCM1-), proliferating (PCM1+ centrosome) and pre-fusion state (PCM1+ NE).

References:

1. **Kirby TJ, Patel RM, McClintock TS, Dupont-Versteegden EE, Peterson CA, and McCarthy JJ**. Myonuclear transcription is responsive to mechanical load and DNA content but uncoupled from cell size during hypertrophy. *Molecular biology of the cell* 27: 788-798, 2016.
2. **Bruusgaard J, Liestøl K, and Gundersen K**. Distribution of myonuclei and microtubules in live muscle fibers of young, middle-aged, and old mice. *Journal of applied physiology* 100: 2024-2030, 2006.

3. **Jakobsen JR, Jakobsen N, Mackey AL, Koch M, Kjaer M, and Krogsgaard MR**. Remodeling of muscle fibers approaching the human myotendinous junction. *Scandinavian journal of medicine & science in sports* 28: 1859-1865, 2018.

4. **Roman W, and Gomes ER**. Nuclear positioning in skeletal muscle. *Seminars in Cell & Developmental Biology* 82: 51-56, 2018.

5. **Murach KA, White SH, Wen Y, Ho A, Dupont-Versteegden EE, McCarthy JJ, and Peterson CA**. Differential requirement for satellite cells during overload-induced muscle hypertrophy in growing versus mature mice. *Skeletal muscle* 7: 1-13, 2017.

6. **Chaillou T, Lee JD, England JH, Esser KA, and McCarthy JJ**. Time course of gene expression during mouse skeletal muscle hypertrophy. *Journal of applied physiology* 2013.

7. **Englund DA, Peck BD, Murach KA, Neal AC, Caldwell HA, McCarthy JJ, Peterson CA, and Dupont-Versteegden EE**. Resident muscle stem cells are not required for testosterone-induced skeletal muscle hypertrophy. *American Journal of Physiology-Cell Physiology* 317: C719-C724, 2019.

8. **Gundersen K**. Muscle memory and a new cellular model for muscle atrophy and hypertrophy. *Journal of Experimental Biology* 219: 235-242, 2016.

9. **Gundersen K, Bruusgaard JC, Egner I, Eftestøl E, and Bengtsen M**. Muscle memory: virtues of your youth? *The Journal of physiology* 596: 4289, 2018.

10. **Goh Q, Song T, Petrany MJ, Cramer AA, Sun C, Sadayappan S, Lee S-J, and Millay DP**. Myonuclear accretion is a determinant of exercise-induced remodeling in skeletal muscle. *Elife* 8: e44876, 2019.

11. **Murach KA, Mobley CB, Zdunek CJ, Frick KK, Jones SR, McCarthy JJ, Peterson CA, and Dungan CM**. Muscle memory: myonuclear accretion, maintenance, morphology, and miRNA levels with training and detraining in adult mice. *Journal of cachexia, sarcopenia and muscle* 2020.

12. **Murach KA, Walton RG, Fry CS, Michaelis SL, Groshong JS, Finlin BS, Kern PA, and Peterson CA**. Cycle training modulates satellite cell and transcriptional responses to a bout of resistance exercise. *Physiological reports* 4: e12973, 2016.

13. **Dungan CM, Murach KA, Frick KK, Jones SR, Crow SE, Englund DA, Vechetti Jr IJ, Figueiredo VC, Levitan BM, and Satin J**. Elevated myonuclear density during skeletal muscle hypertrophy in response to training is reversed during detraining. *American Journal of Physiology-Cell Physiology* 316: C649-C654, 2019.

14. **Psilander N, Eftestøl E, Cumming KT, Juvkam I, Ekblom MM, Sunding K, Wernbom M, Holmberg HC, Ekblom B, Bruusgaard JC, Raastad T, and Gundersen K**. Effects of training, detraining, and retraining on strength, hypertrophy, and myonuclear number in human skeletal muscle. *J Appl Physiol (1985)* 126: 1636-1645, 2019.

15. **Blocquiaux S, Gorski T, Van Roie E, Ramaekers M, Van Thienen R, Nielens H, Delecluse C, De Bock K, and Thomis M**. The effect of resistance training, detraining and retraining on muscle strength and power, myofibre size, satellite cells and myonuclei in older men. *Experimental Gerontology* 133: 110860, 2020.

16. **Seaborne RA, Strauss J, Cocks M, Shepherd S, O'Brien TD, Van Someren KA, Bell PG, Murgatroyd C, Morton JP, and Stewart CE**. Human skeletal muscle possesses an epigenetic memory of hypertrophy. *Scientific reports* 8: 1-17, 2018.

17. **Seaborne RA, Hughes DC, Turner DC, Owens DJ, Baehr LM, Gorski P, Semenova EA, Borisov OV, Larin AK, and Popov DV**. UBR5 is a novel E3 ubiquitin ligase involved in skeletal muscle hypertrophy and recovery from atrophy. *The Journal of physiology* 597: 3727-3749, 2019.

18. **Wen Y, Dungan CM, Mobley CB, Valentino T, von Walden F, and Murach KA**. Nucleus Type-Specific DNA Methylomics Reveals Epigenetic "Memory" of Prior Adaptation in Skeletal Muscle. *Function* 2: zqab038, 2021.

19. **Fisher AG, Seaborne RA, Hughes TM, Gutteridge A, Stewart C, Coulson JM, Sharples AP, and Jarvis JC**. Transcriptomic and epigenetic regulation of disuse atrophy and the return to activity in skeletal muscle. *The Faseb Journal* 31: 5268-5282, 2017.

20. **Folker E, and Baylies M**. Nuclear positioning in muscle development and disease. *Frontiers in physiology* 4: 363, 2013.
21. **Snijders T, Aussieker T, Holwerda A, Parise G, van Loon LJ, and Verdijk LB**. The concept of skeletal muscle memory: Evidence from animal and human studies. *Acta Physiologica* e13465, 2020.
22. **Sakamoto Y**. Histological features of endomysium, perimysium and epimysium in rat lateral pterygoid muscle. *Journal of morphology* 227: 113-119, 1996.
23. **Rowe RWD**. Morphology of perimysial and endomysial connective tissue in skeletal muscle. *Tissue and Cell* 13: 681-690, 1981.
24. **Viggars MR, Wen Y, Peterson CA, and Jarvis JC**. Automated cross-sectional analysis of trained, severely atrophied and recovering rat skeletal muscles using MyoVision 2.0. *Journal of Applied Physiology* 2022.
25. **Wen Y, Murach KA, Jr. IJV, Fry CS, Vickery C, Peterson CA, McCarthy JJ, and Campbell KS**. MyoVision: software for automated high-content analysis of skeletal muscle immunohistochemistry. *Journal of Applied Physiology* 124: 40-51, 2018.
26. **Winje I, Bengtsen M, Eftestøl E, Juvkam I, Bruusgaard JC, and Gundersen K**. Specific labelling of myonuclei by an antibody against pericentriolar material 1 on skeletal muscle tissue sections. *Acta Physiologica* 223: e13034, 2018.
27. **Dammermann A, Müller-Reichert T, Pelletier L, Habermann B, Desai A, and Oegema K**. Centriole assembly requires both centriolar and pericentriolar material proteins. *Developmental cell* 7: 815-829, 2004.
28. **Espigat-Georger A, Dyachuk V, Chemin C, Emorine L, and Merdes A**. Nuclear alignment in myotubes requires centrosome proteins recruited by nesprin-1. *Journal of cell science* 129: 4227-4237, 2016.
29. **Kubo A, Sasaki H, Yuba-Kubo A, Tsukita S, and Shiina N**. Centriolar satellites: molecular characterization, ATP-dependent movement toward centrioles and possible involvement in ciliogenesis. *The Journal of cell biology* 147: 969-980, 1999.
30. **Brunn A**. The complex pericentriolar material 1 protein allows differentiation between myonuclei and nuclei of satellite cells of the skeletal muscle. *Acta Physiologica* 223: e13103, 2018.
31. **Blau HM, Webster C, Pavlath GK, and Chiu C-P**. Evidence for defective myoblasts in Duchenne muscular dystrophy. In: *Gene Expression in Muscle*Springer, 1985, p. 85-110.
32. **Yaffe D, and Saxel O**. Serial passaging and differentiation of myogenic cells isolated from dystrophic mouse muscle. *Nature* 270: 725-727, 1977.
33. **Mackey AL, Rasmussen LK, Kadi F, Schjerling P, Helmark IC, Ponsot E, Aagaard P, Durigan JLQ, and Kjaer M**. Activation of satellite cells and the regeneration of human skeletal muscle are expedited by ingestion of nonsteroidal anti-inflammatory medication. *The FASEB Journal* 30: 2266-2281, 2016.
34. **Mackey AL, and Kjaer M**. The breaking and making of healthy adult human skeletal muscle in vivo. *Skeletal muscle* 7: 24, 2017.
35. **Bergström J**. Percutaneous needle biopsy of skeletal muscle in physiological and clinical research. *Scandinavian journal of clinical and laboratory investigation* 35: 609-616, 1975.
36. **Owens DJ, Messéant J, Moog S, Viggars M, Ferry A, Mamchaoui K, Lacène E, Roméro N, Brull A, and Bonne G**. Lamin-Related Congenital Muscular Dystrophy Alters Mechanical Signaling and Skeletal Muscle Growth. *International Journal of Molecular Sciences* 22: 306, 2021.
37. **Serrano AL, Baeza-Raja B, Perdiguero E, Jardí M, and Muñoz-Cánoves P**. Interleukin-6 is an essential regulator of satellite cell-mediated skeletal muscle hypertrophy. *Cell metabolism* 7: 33-44, 2008.
38. **Schneider CA, Rasband WS, and Eliceiri KW**. NIH Image to ImageJ: 25 years of image analysis. *Nature methods* 9: 671-675, 2012.
39. **Srsen V, Fant X, Heald R, Rabouille C, and Merdes A**. Centrosome proteins form an insoluble perinuclear matrix during muscle cell differentiation. *BMC cell biology* 10: 28, 2009.

40. **Wen Y, Englund DA, Peck BD, Murach KA, McCarthy JJ, and Peterson CA**. Myonuclear transcriptional dynamics in response to exercise following satellite cell depletion. *Iscience* 24: 102838, 2021.
41. **Bergmann O, Zdunek S, Alkass K, Druid H, Bernard S, and Frisén J**. Identification of cardiomyocyte nuclei and assessment of ploidy for the analysis of cell turnover. *Experimental cell research* 317: 188-194, 2011.
42. **Bergmann O, and Jovinge S**. Isolation of cardiomyocyte nuclei from post-mortem tissue. *JoVE (Journal of Visualized Experiments)* e4205, 2012.
43. **Petrany MJ, Swoboda CO, Sun C, Chetal K, Chen X, Weirauch MT, Salomonis N, and Millay DP**. Single-nucleus RNA-seq identifies transcriptional heterogeneity in multinucleated skeletal myofibers. *Nature communications* 11: 1-12, 2020.
44. **Fant X, Srsen V, Espigat-Georger A, and Merdes A**. Nuclei of non-muscle cells bind centrosome proteins upon fusion with differentiating myoblasts. *PLoS One* 4: e8303, 2009.
45. **Gimpel P, Lee YL, Sobota RM, Calvi A, Koullourou V, Patel R, Mamchaoui K, Nédélec F, Shackleton S, and Schmoranzer J**. Nesprin-1α-dependent microtubule nucleation from the nuclear envelope via Akap450 is necessary for nuclear positioning in muscle cells. *Current Biology* 27: 2999-3009. e2999, 2017.
46. **Damas F, Libardi CA, Ugrinowitsch C, Vechin FC, Lixandrão ME, Snijders T, Nederveen JP, Bacurau AV, Brum P, and Tricoli V**. Early-and later-phases satellite cell responses and myonuclear content with resistance training in young men. *PloS one* 13: e0191039, 2018.
47. **Karlsen A, Bechshøft RL, Malmgaard-Clausen NM, Andersen JL, Schjerling P, Kjaer M, and Mackey AL**. Lack of muscle fibre hypertrophy, myonuclear addition, and satellite cell pool expansion with resistance training in 83-94-year-old men and women. *Acta Physiologica* 227: e13271, 2019.
48. **Karlsen A, Couppé C, Andersen JL, Mikkelsen UR, Nielsen RH, Magnusson SP, Kjaer M, and Mackey AL**. Matters of fiber size and myonuclear domain: does size matter more than age? *Muscle & nerve* 52: 1040-1046, 2015.
49. **Snijders T, Nederveen JP, Bell KE, Lau SW, Mazara N, Kumbhare DA, Phillips SM, and Parise G**. Prolonged exercise training improves the acute type II muscle fibre satellite cell response in healthy older men. *The Journal of physiology* 597: 105-119, 2019.
50. **Snijders T, Smeets JS, Van Kranenburg J, Kies A, van Loon L, and Verdijk LB**. Changes in myonuclear domain size do not precede muscle hypertrophy during prolonged resistance-type exercise training. *Acta physiologica* 216: 231-239, 2016.
51. **Snijders T, Wall BT, Dirks ML, Senden JM, Hartgens F, Dolmans J, Losen M, Verdijk LB, and van Loon LJ**. Muscle disuse atrophy is not accompanied by changes in skeletal muscle satellite cell content. *Clinical science* 126: 557-566, 2014.

Figure Legends:

Figure 1: PCM1 localisation in C2C12 myoblast/myotube cultures. **(A)** Following 2 days in LSM, the culture contains both undifferentiated myoblasts which have characteristic PCM1+ centrosomes at the edge of their nucleus(*) and differentiated myotubes(#). **(B)** After 7-days in LSM, few undifferentiated myoblasts remain. Most nuclei are incorporated into multinucleated myotubes and show high PCM1 positivity. Scale bars indicate 50µm. **(C)** Higher magnification imaging of PCM1 localised to the centrosome in the myoblast(*) after 2 days in LSM and **(D)** at the NE in the myotube(#) after 7 days in LSM. Scale bars indicate 25µm. **(E)** PCM1 localisation as a % of total DAPI+ nuclei after 2-days in LSM. **(F)** PCM1 localisation as a % of total DAPI+ nuclei after 7-days in LSM.

Figure 2: Cross-sections from control human muscle **(A)** illustrates the PCM1+ NE of transversely sectioned myonuclei associated with the myofiber border(m). Some nuclei within the endomysium have PCM1 staining at the centrosome(*) and NE(#). Pax7+ cells also exhibit PCM1 positivity at the centrosome even in control tissue(α). **(B)** Normal distribution of myonuclei in a control fiber with PCM1+ Nes. **(C)** A control human myofiber exhibiting a Pax7+ cell that is also PCM1+(α) alongside a myonucleus(m). Scale bars indicate 80µm. **(D)** The number of Pax7+ cells present per muscle fiber. **(E)** The number of proliferating Pax7+ cells (PCM1+ centrosome) following damage caused by forced eccentric contractions. Data is presented from 100 SCs for each participant per timepoint, counted on 32 ± 8 muscle fibers (control), 27 ± 3 muscle fibers (2 days), 17 ± 6 muscle fibers (7 days) and 24 ± 3 muscle fibers (30 days). The number of SCs was not normalized to fiber length which we note likely differed across extracted fibers. Significant differences are displayed as follows, $P < 0.05$*, $P < 0.01$**, $P < 0.001$***.

Figure 3: Single human myofibers extracted 7 days post eccentric damage. **(A, B)** show 3 myofibers at different positions within a z-stack. The right most fiber is necrotic, indicated by infiltration of a dense population of nuclei belonging to proliferating macrophages with PCM1+ centrosomes(*). Several myonuclei have been highlighted with their distinctive PCM1+ NE (#). Scale bars indicate 100µm.

Figure 4: Human cross-sections from biopsies 7 days post eccentric damage. **(A, B)**. Large bodies of proliferating immune cells can be observed in necrotic zones and regenerating fibers identified through PCM1+

centrosomes(*), alongside myonuclei(m) and PCM1+ Pax7+ cells(α). **(C)** confirms that macrophages are PCM1+ inside and around myofibers through CD68 labelling. Scale bars indicate 80µm.

Figure 5: Cross sections showing morphology of WT and Lmna$^{+/\Delta K32}$ mouse plantaris muscle. **(A)** WT muscle, 7 days post a sham operation. **(B)** WT muscle 7 days post functional overload displays an increase in fiber cross-sectional area in comparison to the sham operated muscles. **(C)** Lmna$^{+/\Delta K32}$ muscle 7 days post a sham operation. **(D, E)** Lmna$^{+/\Delta K32}$ muscle 7 days post functional overload shows excessive dystrophin protein in regenerating areas with myofibres/myotubes containing centralised nuclei with a PCM1+ nuclear envelope. Scale bars indicate 50µm.

Figure 6: (A) Single extracted myofiber from WT sham operated mouse showing PCM1+ centrosome labelling around a single Pax7+ cell(α). Scale bars indicate 20µm. **(B)** PCM1 labels the NE of newly differentiated myonuclei during nuclear spreading following 1-week of functional overload in the WT mouse. PCM1 also labels a Pax7+ cell between an adjacent mature fiber(α). Scale bars indicate 50µm. **(C)** Single extracted myofiber from a sham operated *Lmna*$^{+/\Delta K32}$ mouse, (α) is indicative of satellite cells. Scale bars indicate 50µm. **(D)** *Lmna*$^{+/\Delta K32}$ fibers following 1 week of functional overload with a number of Pax7+ cells and centrally located myonuclei Scale bars indicate 20µm. **(E)** *Lmna*$^{+/\Delta K32}$ intact myofibers adjacent to an early myocyte/myofiber following 1-week of functional overload. We note this was more frequent in the *Lmna*$^{+/\Delta K32}$ mutants after overload compared to the WT. The nuclei appear to be in the alignment stage of myogenesis. Scale bars indicate 20µm. **(F)** Number of Pax7+ cells per fiber across all conditions (not normalised to fiber length), including number of fibers assessed per individual. **(G)** WT and *Lmna*$^{+/\Delta K32}$ have similar levels of Pax7+ cells with PCM1+ centrosomes which is elevated following 1-week of functional overload. Data is presented from 100 SCs each, counted on 39 ± 3 muscle fibers (WT sham), 52 ± 7 muscle fibers (*Lmna*$^{+/\Delta K32}$ Sham), 36 ± 4 muscle fibers (WT 1-week overload) and 41 ± 7 muscle fibers (*Lmna*$^{+/\Delta K32}$ 1-week overload). *Indicates statistical significance between conditions ($P < 0.05$).

Supplementary Figure 1: Bland-Altman plot analysis comparing PCM1 labelling of myonuclei (subsarcolemmal PCM1) to manual quantification of myonuclei through their subsarcolemmal positioning in control and 7-days post damage on human transverse cross-sections.

534 **Supplementary Figure 2:** Bland-Altman plot analysis comparing myonuclei per fiber cross-section
535 measurements to manual quantification of all PCM1+ nuclei for WT & $LMNA^{+/\Delta K32}$ control mice and after
536 functional overload.

F1

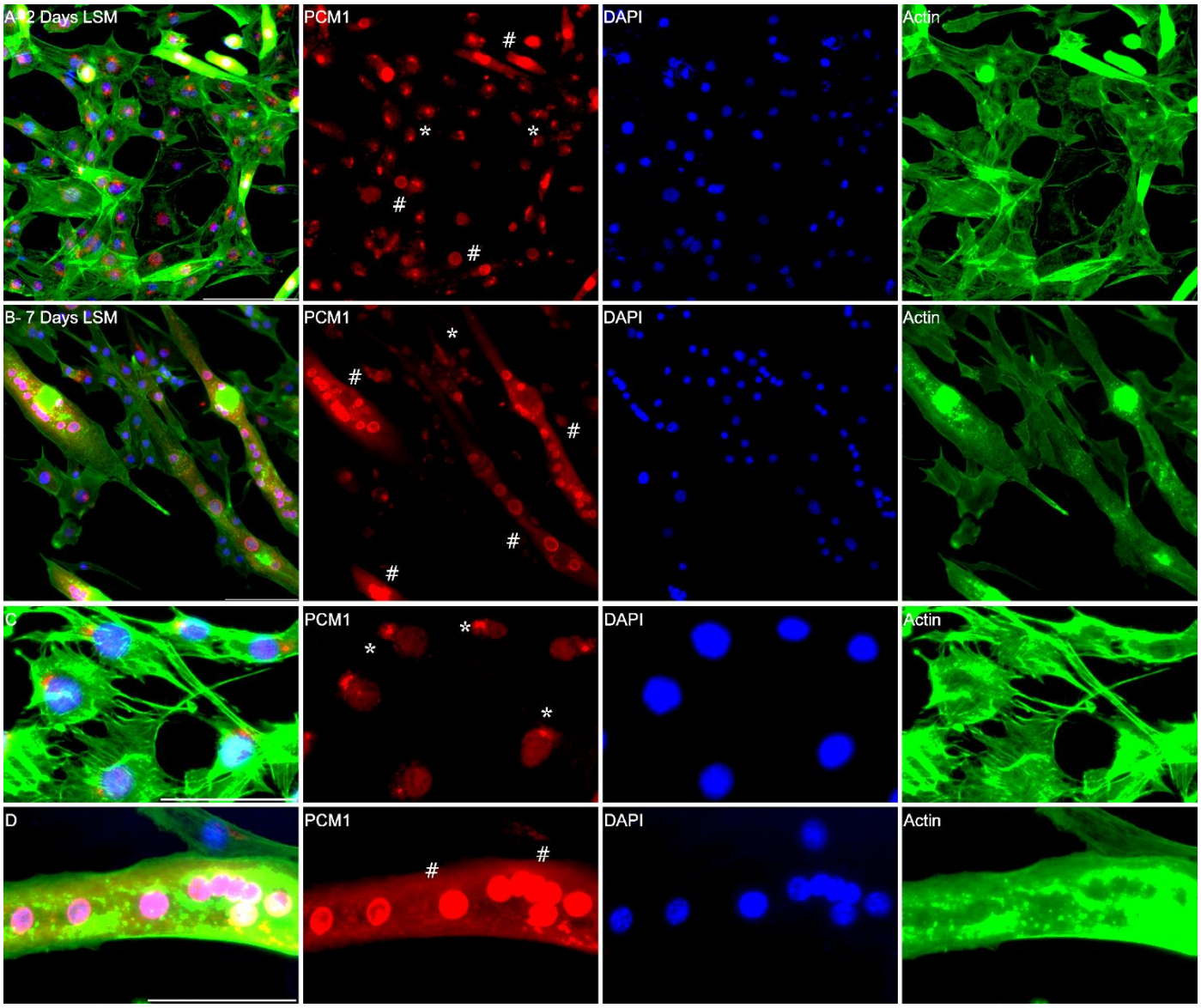
A- 2 Days LSM
PCM1
DAPI
Actin
B- 7 Days LSM
PCM1
DAPI
Actin
C
PCM1
DAPI
Actin
D
PCM1
DAPI
Actin

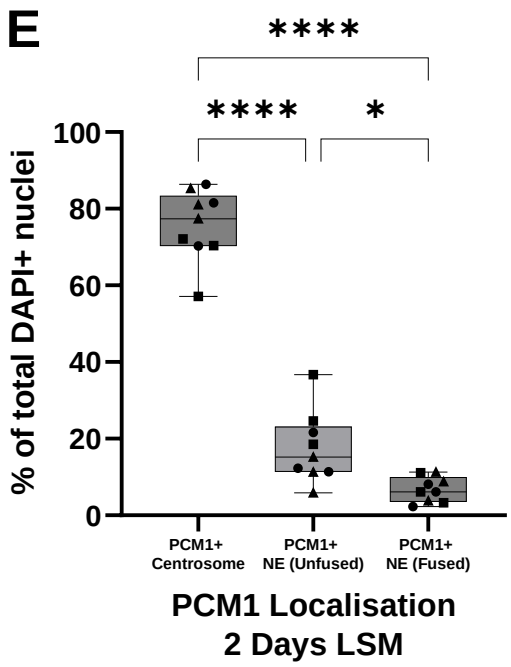
E
****
****
*
% of total DAPI+ nuclei
100
80
60
40
20
0
PCM1+ Centrosome
PCM1+ NE (Unfused)
PCM1+ NE (Fused)
PCM1 Localisation
2 Days LSM

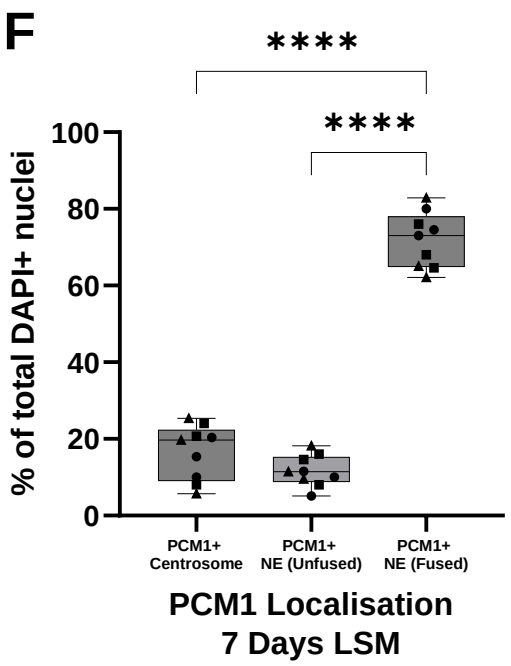
F
****
****
% of total DAPI+ nuclei
100
80
60
40
20
0
PCM1+ Centrosome
PCM1+ NE (Unfused)
PCM1+ NE (Fused)
PCM1 Localisation
7 Days LSM

F2

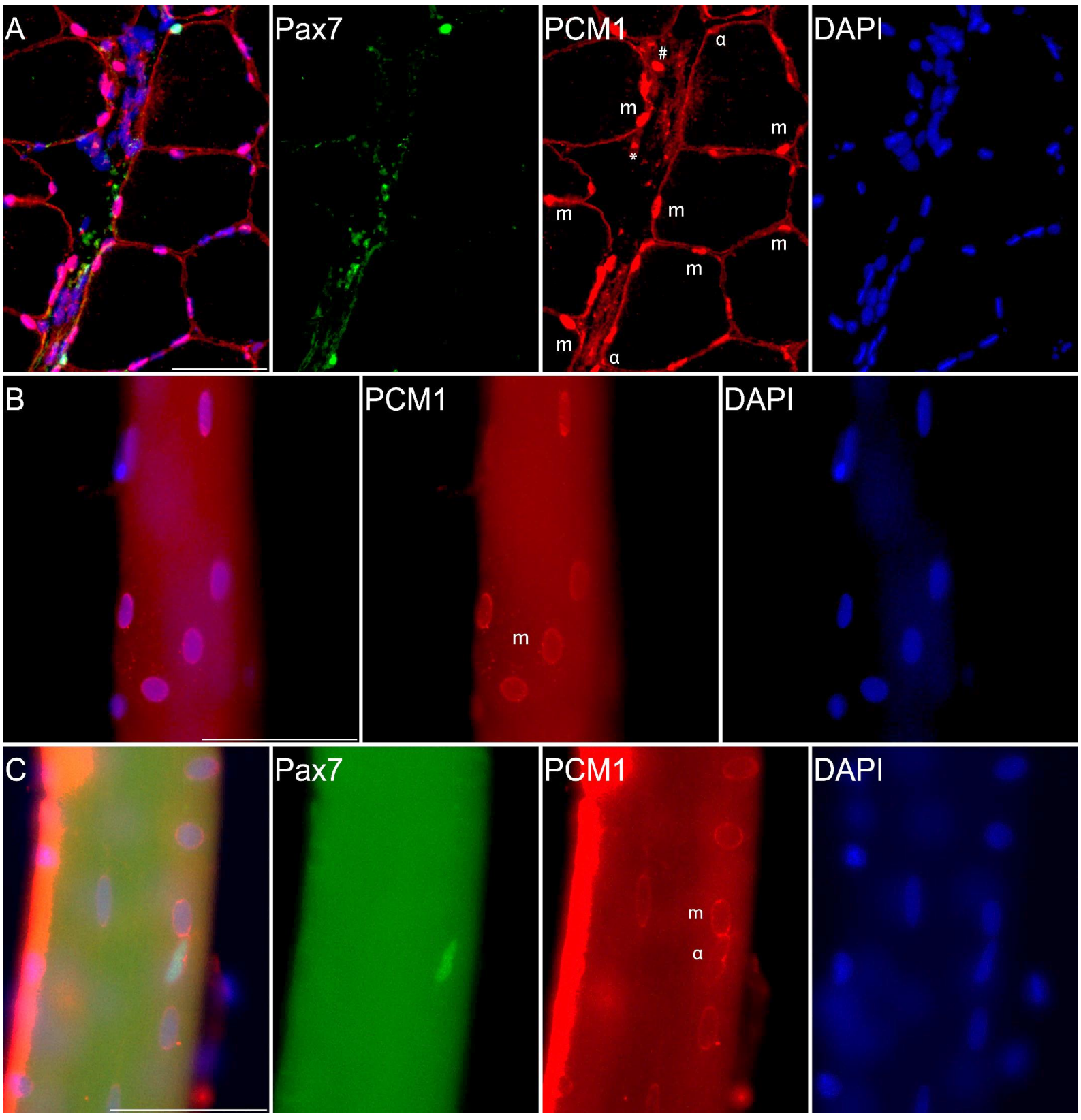
A
Pax7
PCM1
DAPI
#
α
m
*
B
C
D
E
Pax7+ cells per fiber
***
**
Control
2 Days
7 Days
30 Days
P1: 40 fibers
P2: 24 fibers
P1: 30 fibers
P2: 25 fibers
P1: 11 fibers
P2: 23 fibers
P1: 27 fibers
P2: 21 fibers
% of Pax7+ cells with PCM1 positivity
*

T1

Per Fiber Cross Section	Control	7 Days Post Damage	*P*-Value
Pax7+ Nuclei	0.16 ± 0.03	0.17 ± 0.04	0.7
Pax7+/PCM1+	0.06 ± 0.02	0.09 ± 0.01	**0.036***
Manually Counted Myonuclei (DAPI + Sarcolemmal Positioning)	2.04 ± 0.15	2.01 ± 0.08	0.827
PCM1+ Myonuclei	2.1 ± 0.17	2.16 ± 0.08	0.679
Total PCM1+ Nuclei	2.92 ± 0.5	3.89 ± 0.84	0.094
Total DAPI + Nuclei	4.43 ± 0.94	7.03 ± 2.27	**0.048***

F3

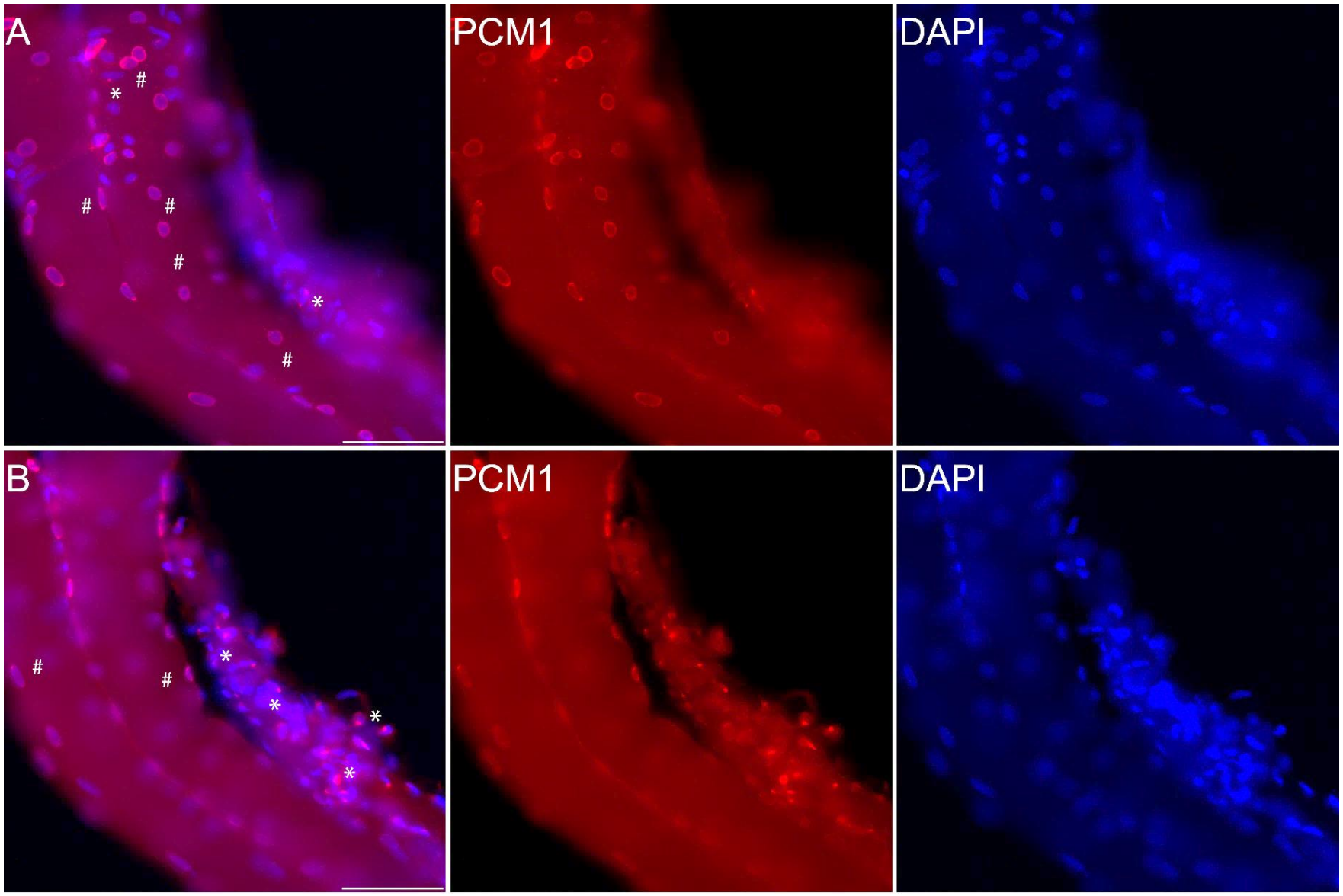

F4

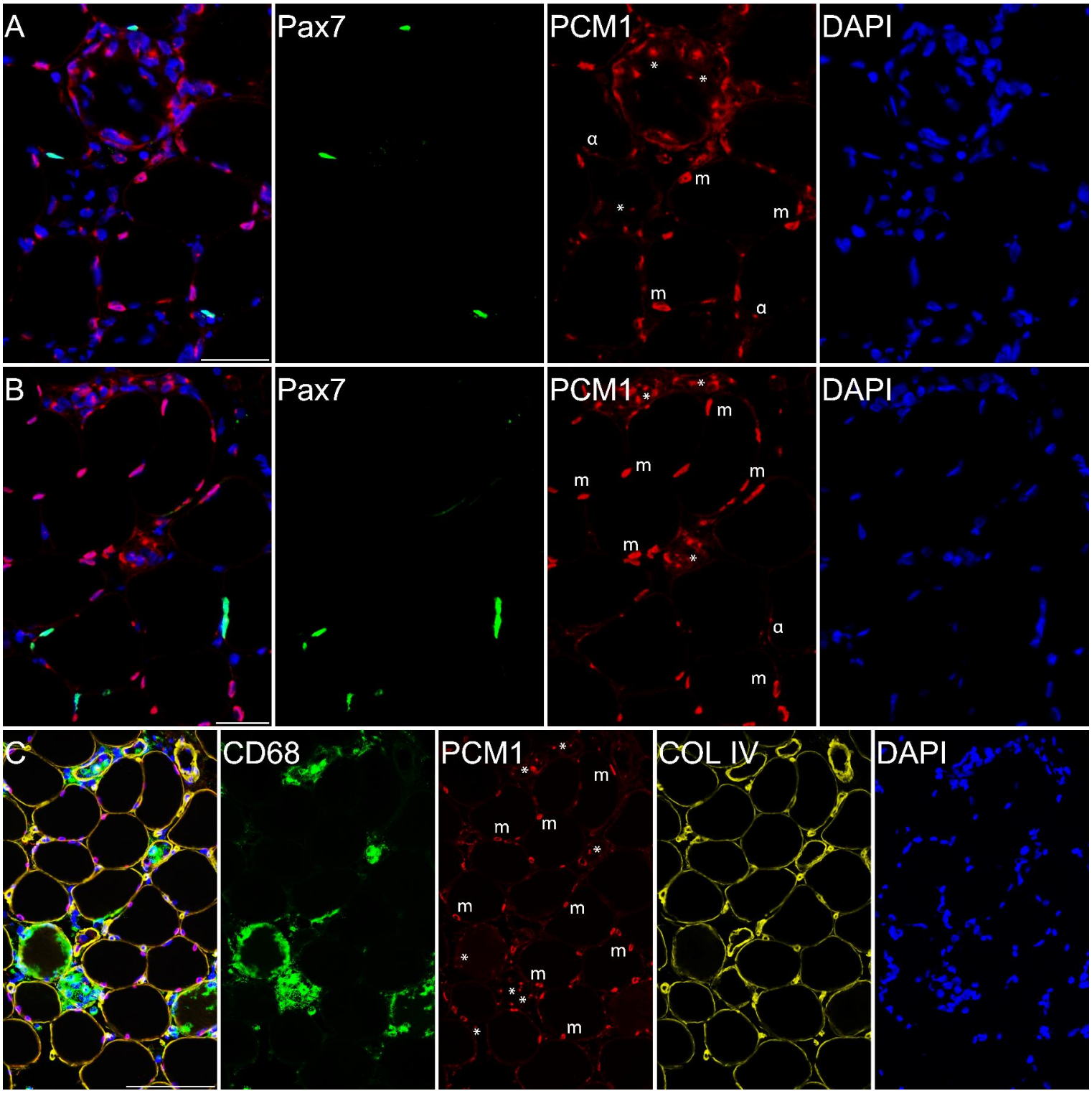

F5

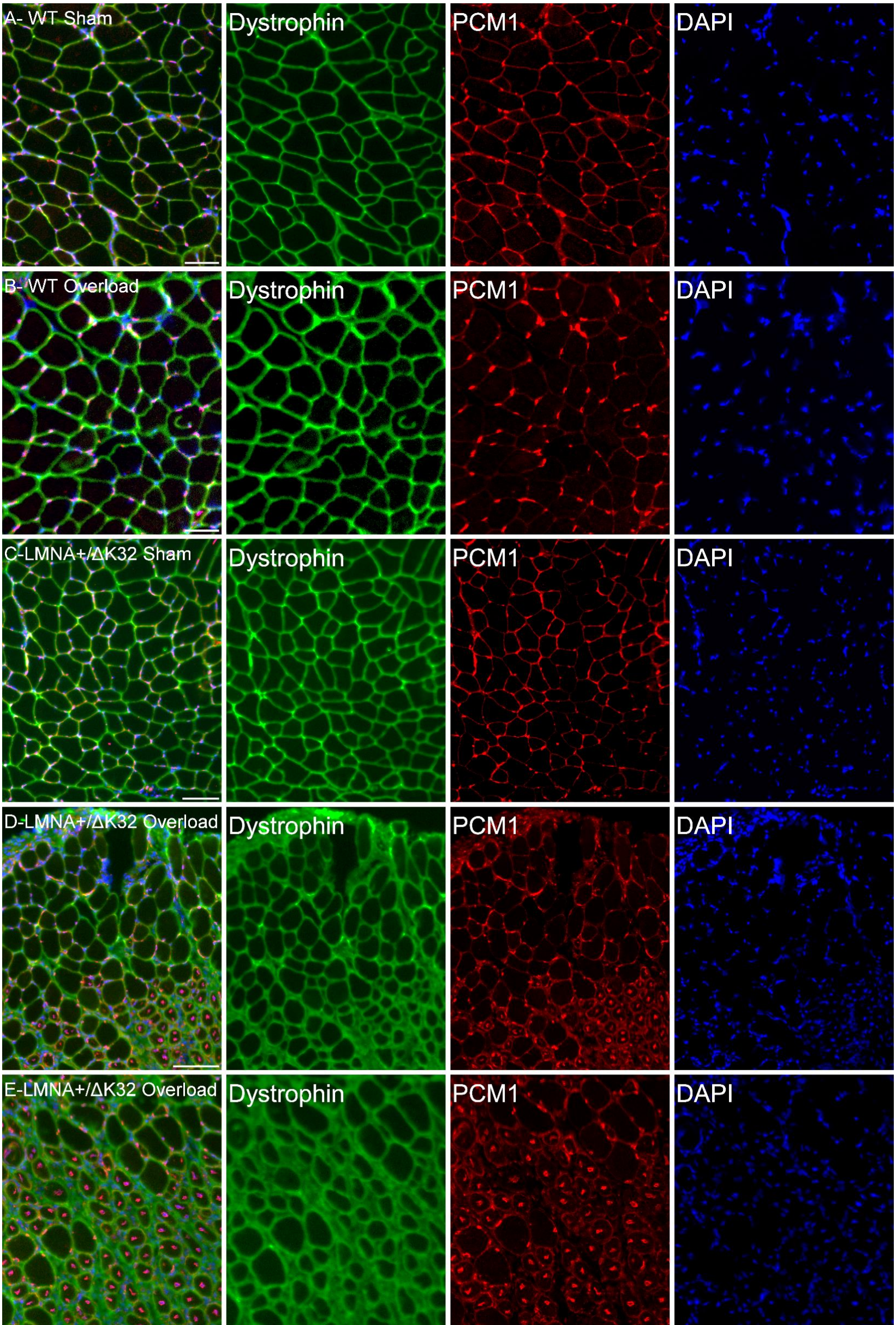
A- WT Sham
Dystrophin
PCM1
DAPI
B- WT Overload
Dystrophin
PCM1
DAPI
C-LMNA+/ΔK32 Sham
Dystrophin
PCM1
DAPI
D-LMNA+/ΔK32 Overload
Dystrophin
PCM1
DAPI
E-LMNA+/ΔK32 Overload
Dystrophin
PCM1
DAPI

F6

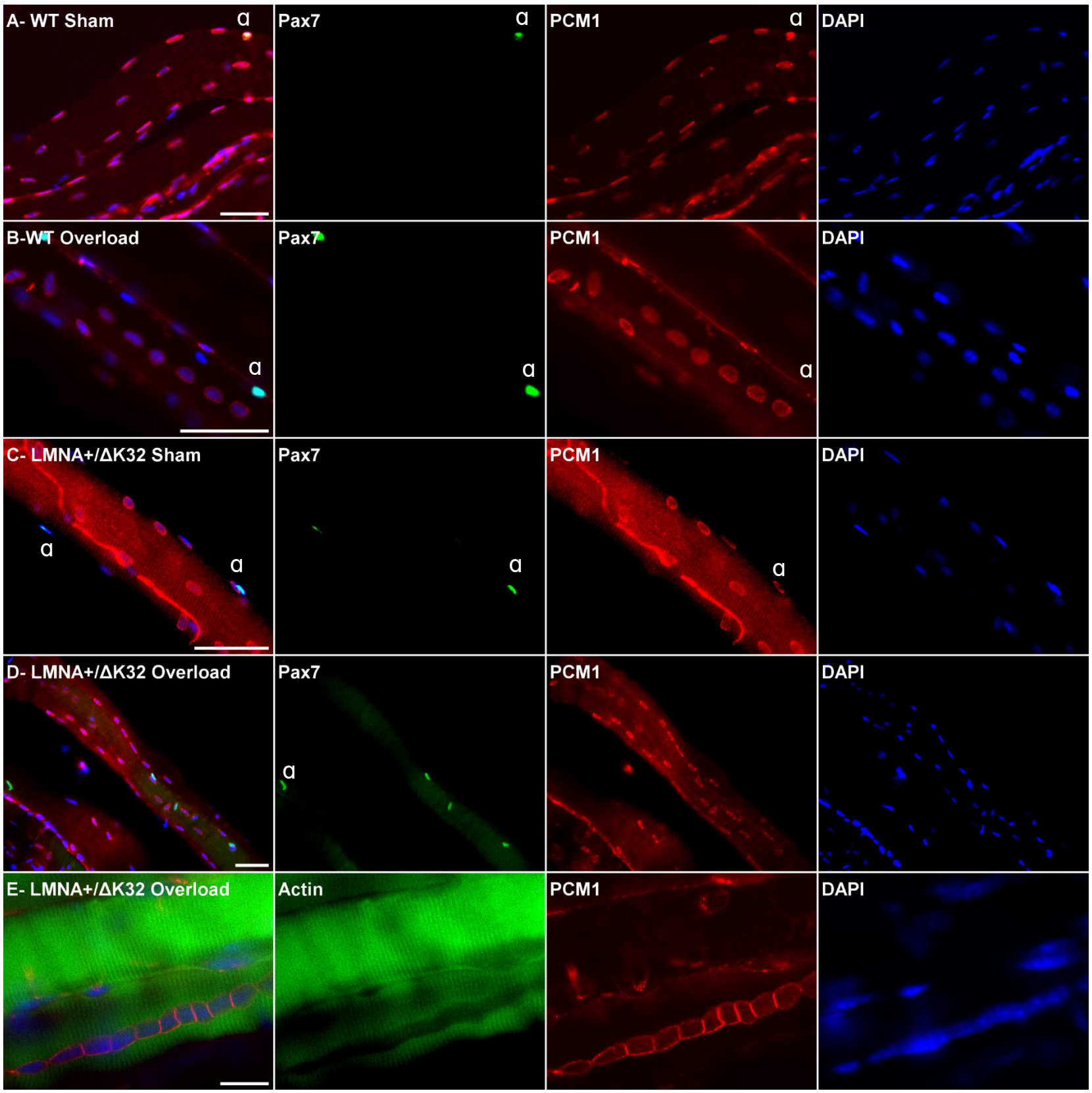
A- WT Sham
Pax7
PCM1
DAPI
B-WT Overload
C- LMNA+/ΔK32 Sham
D- LMNA+/ΔK32 Overload
E- LMNA+/ΔK32 Overload
Actin
a

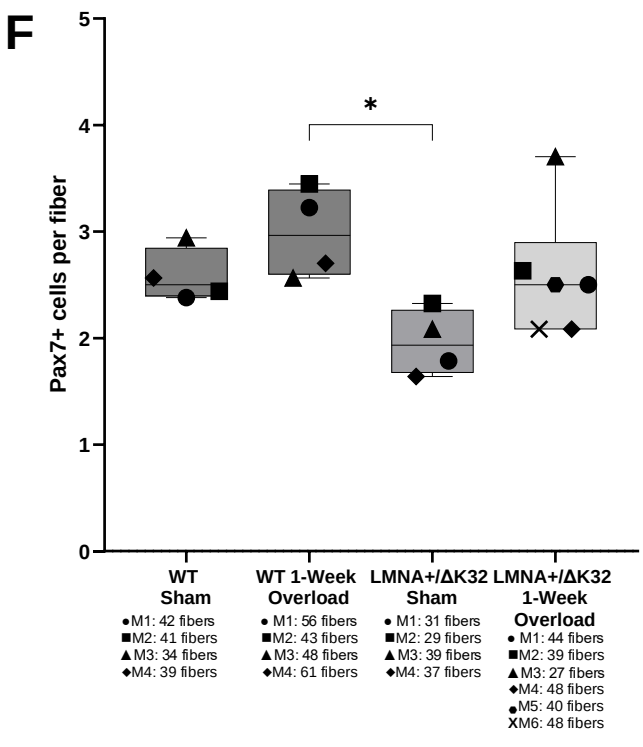
F
Pax7+ cells per fiber
*
WT Sham
●M1: 42 fibers
■M2: 41 fibers
▲M3: 34 fibers
◆M4: 39 fibers
WT 1-Week Overload
● M1: 56 fibers
■M2: 43 fibers
▲M3: 48 fibers
◆M4: 61 fibers
LMNA+/ΔK32 Sham
● M1: 31 fibers
■M2: 29 fibers
▲M3: 39 fibers
◆M4: 37 fibers
LMNA+/ΔK32 1-Week Overload
● M1: 44 fibers
■M2: 39 fibers
▲M3: 27 fibers
◆M4: 48 fibers
●M5: 40 fibers
XM6: 48 fibers

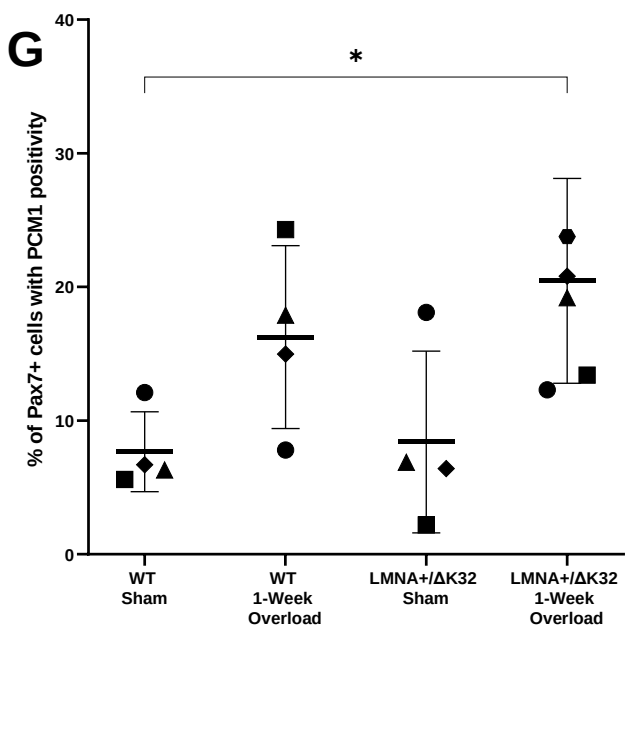
G
% of Pax7+ cells with PCM1 positivity
*
WT Sham
WT 1-Week Overload
LMNA+/ΔK32 Sham
LMNA+/ΔK32 1-Week Overload

S1

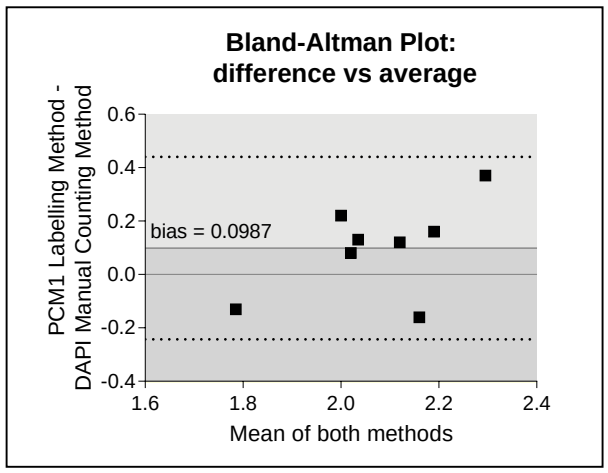

Supplementary Figure 1: Bland-Altman plot analysis comparing PCM1 labelling of myonuclei (subsarcolemmal PCM1) to manual quantification of myonuclei through their subsarcolemmal positioning in control and 7-days post damage on human transverse cross-sections.

S2

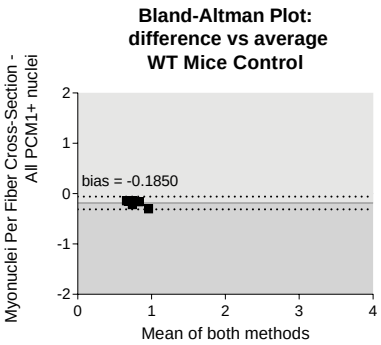

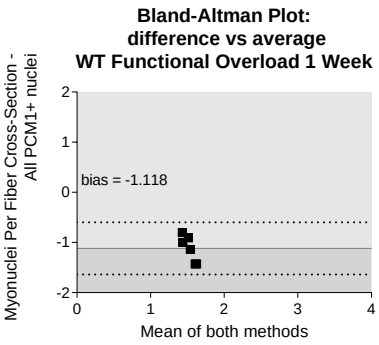

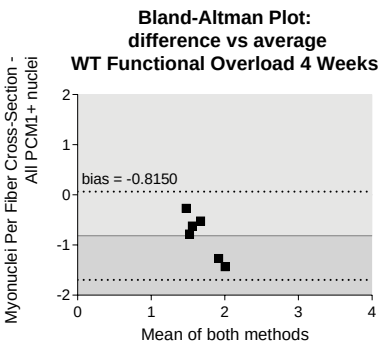

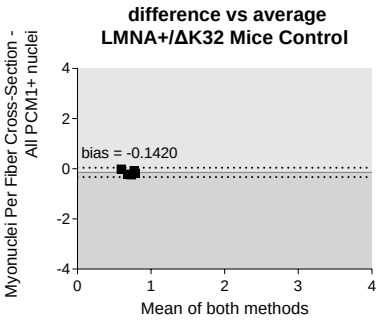

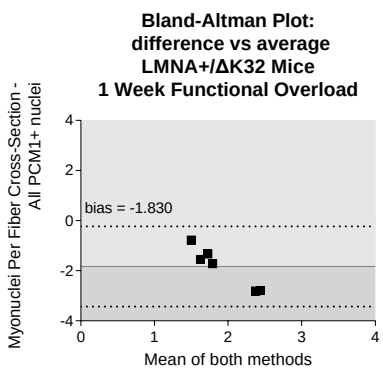

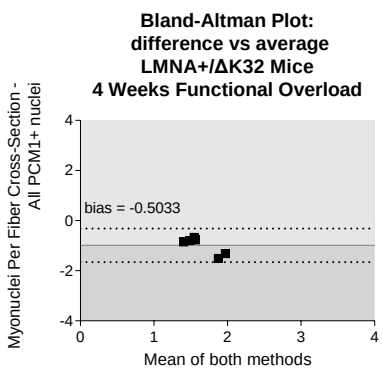

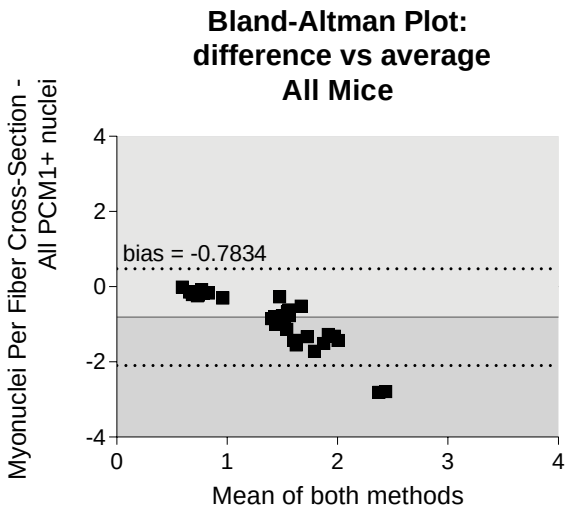

Supplementary Figure 2: Bland-Altman plot analysis comparing myonuclei per fiber cross-section measurements to manual quantification of all PCM1+ nuclei for WT & LMNA$^{+/\Delta K32}$ control mice and after functional overload.